The definitive version is published in *Nature* **517**, 68-72 (01 January 2015);

doi: 10.1038/nature 14060

Anisotropic hydrogel with embedded electrostatic repulsion among cofacially oriented 2D electrolytes

Mingjie Liu[1], Yasuhiro Ishida[1]*, Yasuo Ebina[2], Takayoshi Sasaki[2], Takaaki Hikima[3], Masaki Takata[3] and Takuzo Aida[1,4]*

[1] *RIKEN Center for Emergent Matter Science, 2-1 Hirosawa, Wako, Saitama 351-0198, Japan.*

[2] *National Institute for Materials Science, International Center for Materials Nanoarchitectonics, 1-1 Namiki, Tsukuba, Ibaraki 305-0044, Japan.*

[3] *RIKEN SPring-8 Center, 1-1-1 Kouto, Sayo, Hyogo 679-5198, Japan.*

[4] *Department of Chemistry and Biotechnology, School of Engineering, The University of Tokyo, 7-3-1 Hongo, Bunkyo-ku, Tokyo 113-8656, Japan.*

In machine technology, levitation devices using magnetically or electrostatically 'repulsive' forces have been put into practical use for maglev trains, vehicle suspensions, noncontact bearings and so forth[1,2]. However, for the design of structural materials, 'repulsive' forces have never been utilized. For example, many polymers-based structural materials are developed by composition with inorganic fillers for enhancing attractive interactions among constituents. Nevertheless, in nature, articular cartilage in animal joints utilizes an electrostatically 'repulsive' force for insulating interfacial mechanical friction even under high compression, to lubricate sliding motions between articular tissues in contact[3,4]. Here we report an anisotropic hydrogel whose mechanical properties are dominated by 'embedded electrostatic repulsion'. This hydrogel resulted from our unexpected finding that negatively charged unilamellar titanate nanosheets[5] in an aqueous colloidal dispersion magnetically align cofacially, where the theory predicts the emergence of maximal electrostatic repulsion among the nanosheets[6]. For minimizing the consequent thermodynamic instability, the aqueous dispersion adopts a quasi-crystalline structural order[7,8], wherein a uniformly large face-to-face nanosheet separation develops up to a macroscopic length scale. This magneto-induced temporal structural ordering can be fixed by transforming the dispersion into a hydrogel[9,10] by in-situ vinyl polymerization initiated with hydroxyl radicals generated upon photoexcitation of the nanosheets[11]. The 'anisotropic electrostatics' thus embedded allows easy deformation of the hydrogel along a shear force applied parallel to the 2D electrolyte plane but makes it resistive against a compressive force applied orthogonally. This mechanical anisotropy becomes more remarkable when additional nanosheets are doped. Before the present work, no 2D inorganic electrolytes were known to align cofacially in a magnetic flux[12–19]. The idea of using 'embedded anisotropic electrostatics', inspired by articular cartilage, may open new possibilities in the development of soft materials.

As an extension of our previous study on highly water-rich hydrogels (aqua materials) supported by a 3D supramolecular network composed of clay nanosheets (Laponite XLG)[20,21], we were interested in utilizing metal oxide nanosheets instead of the clay family for tailoring functional supramolecular hydrogels. As a potential candidate, we chose unilamellar titanate(IV) nanosheet TiNS (Fig. 1b and Supplementary Fig. 1a), which was developed by one of the coauthors[5]. This particular nanosheet consists only of surface atoms adopting a single-crystal-like 2D array and is therefore ultrathin (0.75 nm). It is also characterized by an exceptionally high aspect ratio (~10^4). TiNS is negatively charged and wrapped by tetramethylammonium (Me_4N^+) counterions to furnish an electric double layer in aqueous media. Owing to its large specific surface area and high charge density, TiNS can be well dispersed in aqueous media without dispersants. This unilamellar titanate nanosheet is semiconducting and photocatalytically produces hydroxyl radicals when irradiated in aqueous media with ultraviolet light (λ ~260 nm) (Fig. 1d)[11]. Recently, we reported that an aqueous colloidal dispersion of TiNSs can be photochemically transformed into a hydrogel by in-situ radical polymerization of acrylamide derivatives[11]. In this case, TiNS not only serves as the photocatalyst but also adheres to and non-covalently connects the resulting polymer chains to produce a crosslinked hydrogel network. In the course of this study, we found that colloidally dispersed TiNSs align cofacially in a superconducting magnet. We later noticed that this unprecedented orientation generates a particular electrostatics in a colloidal dispersion. Suppose that two electrically charged 2D sheets are positioned in close proximity to one another in a highly dielectric medium such as water, electrostatic repulsion acts between them, wherein the repulsive force changes as a function of the dihedral angle of the 2D sheets. Most importantly, as illustrated in Fig. 1a[6], the repulsive force becomes maximal when the dihedral angle is 0° (cofacial orientation).

Magnetic orientation is a classical method for orienting 1D and 2D anisotropic objects in a non-contact and nondestructive manner[22,23]. However, only a few studies have been reported for the magnetic orientation of metal oxide nanosheets[12–14]. The most extensively studied is diamagnetic niobate(V) nanosheet NbNS (Fig. 1c and Supplementary Fig. 1b)[12,13], which directs its in-plane orientation vector parallel to the applied magnetic flux (Fig. 2b). Nanosheets scatter light to varying extents depending on their relative orientation to the incident light. As shown in Fig. 2d, when no magnetic field was applied, an aqueous dispersion containing 0.4 wt% NbNS exhibited an optical transmittance of 22% at 450 nm (broken line). When the dispersion was put into a 10-T magnet with its magnetic flux directed orthogonal to the incident light (⊥), the optical transmittance fell off to 18%. When the magnetic flux was then directed parallel (//) to the incident light, the optical transmittance increased from 18% to 27%. The observed magneto-responsive change in optical transmittance is reasonable considering the reported orientation of NbNS in a magnetic field (Fig. 2b)[12,13]. On the contrary, TiNS orients its 2D plane orthogonal to the applied magnetic flux (Fig. 2a), so that its colloidal dispersion displayed a totally opposite magneto-responsive change in optical transmittance (Fig. 2c). Furthermore, the optical transmittance varied more remarkably (67% (⊥)–13% (//); Fig. 2c and Supplementary Figs 4a, 4c) than that of the NbNS dispersion (Fig. 2d and Supplementary Figs 4b, 4d). Although magnetically oriented NbNSs are not mutually cofacial and freely rotatable around the orientation vector (Fig. 2b)[12,13], cofacially oriented TiNSs in a magnetic flux, as described later, form a layered structure with a quasi-crystalline order (Fig. 2a). This particular structural ordering develops up to a macroscopic length scale and gives rise to the large optical anisotropy shown in Fig. 2c. SQUID measurements indicated that both TiNS and NbNS are diamagnetic (Supplementary Fig. 3). We confirmed that their orientation directions are consistent with those predicted by

a theory established for diamagnetic species (Supplementary Fig. 2 and Supplementary Table 2)[24].

When the applied magnetic field was attenuated from 10 T, the TiNS dispersion began to lose its optical anisotropy at < 4 T due to thermal structural relaxation (Supplementary Fig. 5). However, this relaxation was completely prevented by gelating the dispersion (Fig. 3a)[17,19,25], where the structural anisotropy could be seen by the naked eye (Fig. 3b). As already described, photoexcited TiNSs (λ ~260 nm) in water catalytically generate hydroxyl radicals capable of in-situ initiating the polymerization of acrylamide derivatives[11]. The resultant polymer chains adhere to TiNSs and crosslink to form a 3D network, thereby forming a supramolecular hydrogel. In the present work, we used a small amount of an organic crosslinker (Fig. 1d) to tune the mechanical properties of the hydrogel (Supplementary Information, Section 4). As shown in Fig. 3b, the resultant hydrogel looked opaque when viewed along the applied magnetic flux (i) but exhibited high optical transparency when viewed from its orthogonal directions (ii and iii).

Of particular interest, when the optically anisotropic hydrogel (TiNS; 0.6 wt%) was exposed to a synchrotron X-ray beam parallel to the TiNS plane, the resultant 2D small-angle X-ray scattering (SAXS) profile displayed a linear array of multiple diffuse spots up to the (500) face (Fig. 3c, ii). In contrast, when the incident X-ray beam was directed orthogonal to the TiNS plane, only a single diffuse spot resulted (Fig. 3c, i). A detailed SAXS analysis revealed that TiNSs align with a uniform plane-to-plane separation of 35.5 nm (Fig. 3c, ii). This separation expanded further to 52.4 nm upon two-fold dilution of the dispersion (TiNS; 0.3 wt%) prior to the gelation. However, upon further dilution to 0.1 wt%, the diffuse spots turned obscure (Fig. 3d and Supplementary Fig. 6), indicating that the critical volume fraction

of TiNSs for the formation of such an uniformly spaced layered structure is approximately 0.03 vol%. As determined from the scattering intensity–azimuthal angle plots (Supplementary Fig. 6), the degree of orientation is remarkably high with an order parameter of 0.96[26]. Considering that TiNS is negatively charged and wrapped by Me_4N^+ counterions to furnish an electric double layer, this quasi-crystalline structural order is most likely caused by electrostatic repulsion among the cofacially oriented TiNSs. As already discussed in Fig. 1a (left), the inter-plane electrostatic repulsion is maximal when the TiNSs are cofacial to one another[6]. So, in order to minimize the resultant thermodynamic instability, the cofacially oriented 2D electrolytes adopt a uniformly large face-to-face separation, resulting in a quasi-crystalline structural order[7,8]. Accordingly, when an electrolyte such as Me_4NOH (24 mM) was added to a 0.8 wt% TiNS dispersion, the internal electrostatic repulsion was screened[27], and so the plane-to-plane separation fell off remarkably from 29.7 nm to 9.3 nm (Fig. 3e and Supplementary Fig. 7). Taking into account a large extent of 'contact ion pairing' on the TiNS surface with Me_4N^+, as indicated by a zeta potential analysis (Supplementary Table 1), the observed nanosheet distances in Figs 3d and 3e appear to obey the theory of Debye length (Supplementary Fig. 8c). Water as a highly dielectric medium is essential for the formation of such a long-range structural order, because the SAXS pattern became quite ambiguous when a lower-dielectric medium composed of water and ethylene glycol (50:50 in v/v) was used for the gelation (Supplementary Fig. 9).

We conjectured that our magnetically structured hydrogel may serve for vibration isolation[1,2]. Considering its 'embedded anisotropic electrostatics', the hydrogel might resist against a compressive force applied orthogonal to the TiNS plane (Fig. 4a, left), yet readily deform along a shear force applied parallel to the TiNS plane (Fig. 4b, right). To test this possibility, we prepared three cylindrical pillars (Fig. 4g; 20 mm in diameter and height)

using a magnetically structured hydrogel, where cofacially oriented TiNSs (0.8 wt%) aligned parallel to the cylinder cross-section. On a mechanical oscillator, these pillars were positioned 40 mm apart in a triangular geometry to support a glass stage (130 mm in diameter, 5 mm in thickness and 160 g in weight) featuring at its center a metal sphere (30 mm in diameter and 40 g in weight) on a tee. Then, a large oscillatory motion was continuously applied to the glass stage. As shown in Supplementary Video 1, the cylindrical pillars deformed mostly horizontally in a restricted manner. Consequently, the upper glass stage was kept untilted and moved only slightly from the initial coordinates, thereby allowing for the metal sphere to stay on the tee. In sharp contrast, when embedded TiNSs (0.8 wt%) were oriented orthogonal to the cylinder cross-section (Fig. 4h and Supplementary Video 2) or randomly (Supplementary Video 3), unrestricted deformations of the cylindrical pillars took place to generate large irregular turbulences for the upper glass stage. Here we emphasize that only a tiny amount of 2D electrolytes, depending on their orientation in the pillars, gives rise to such totally different behaviors for vibration isolation.

In order to confirm whether the observed vibration isolation in Fig. 4g indeed originates from the ‘embedded anisotropic electrostatics’, we performed in-depth testing of the mechanical properties of a hydrogel containing cofacially oriented TiNSs (0.8 wt%). This hydrogel, upon compression, displayed a stress–strain curve typical of hydrogels (Fig. 4c). However, its stress profile is clearly dependent on the direction of the compressive force applied to the material. When the hydrogel was compressed orthogonal ($\perp$) to the TiNS plane, its tangent elastic modulus ($E_{\perp}$) became 66 kPa at 40% strain, which is 2.6 times greater than that when compressed parallel (//) to the TiNS plane ($E_{//}$ = 25 kPa). $E_{\perp}$ gradually increased with the content of TiNS ([TiNS]), whereas $E_{//}$ appeared to reach a plateau. Consequently, the gap between $E_{\perp}$ and $E_{//}$, as a measure of mechanical anisotropy, became

larger as [TiNS] increased (Fig. 4e and Supplementary Figs 10a, 10c). Rheological properties of the structured hydrogel also showed an anisotropic feature (Fig. 4d). The hydrogel, when sheared parallel (//) to the TiNS plane, displayed a storage modulus ($G'_{//}$) of 0.6 kPa, which is only one fourth the modulus when the same hydrogel sample was sheared orthogonal ($\perp$) to the TiNS plane ($G'_{\perp}$ = 2.2 kPa). Accordingly, when no weight was applied, a hydrogel cylinder containing horizontally oriented TiNSs (0.8 wt%), upon oscillation, deformed at its free edge much more than a cylinder containing vertically oriented TiNSs (Supplementary Video 4). Similar to the case of compression testing (Fig. 4e and Supplementary Figs 10a, 10c), $G'_{\perp}$ monotonically increased with [TiNS]. However, to our surprise, $G'_{//}$, which initially increased with [TiNS], started to fall off after [TiNS] exceeded around 0.2 wt% (Fig. 4f and Supplementary Figs 10b, 10d). Because TiNSs in the hydrogel serve as crosslinking points[11], the initial increase in $G'_{//}$ with [TiNS] seems quite reasonable. So why does $G'_{//}$ fall off after [TiNS] exceeds around 0.2 wt%? We suppose that, after this critical TiNS concentration, the electrostatic repulsion among the cofacially oriented TiNSs becomes dominant in determining $G'_{//}$. The anisotropy factor in loss moduli ($G''_{\perp}/G''_{//}$) of ~7.0 also supports that this particular electrostatics insulates the internal mechanical friction anisotropically (Supplementary Fig. 11). Over a wide range of the applied frequency and strain, such a large rheological anisotropy in G' and G'' was maintained, thereby accounting for the excellent performance of our hydrogel as a vibration isolator (Supplementary Video 1). Naturally, a hydrogel containing randomly oriented TiNSs did not exhibit anisotropic mechanical properties (Supplementary Fig. 12). The same holds true when the hydrogel network consists of magnetically oriented but non-cofacial NbNSs (Supplementary Fig. 13). We also found that hydrogels prepared in lower dielectric media such as water/ethylene glycol (50:50 in v/v) (Supplementary Fig. 14) and water containing externally added Me_4NOH (24 mM) (Supplementary Fig. 15) carry a poor mechanical anisotropy. These

results are reasonable considering that the electrostatic repulsion does not operate efficiently in these media (Figs 3d, 3e).

Contrary to a preconceived notion that doped fillers always enhance internal frictions of materials[19,28,29], 2D electrolyte fillers, upon cofacial orientation in hydrogels, allow internal frictions to be attenuated and enhanced at the same time at right angles to one another, thereby enabling an excellent performance for vibration isolation. Compared with rubber-based anti-vibration materials mechanically laminated with multiple metal plates, our hydrogel with 'embedded anisotropic electrostatics' is readily processable mostly with water for sustainability. By changing the amounts of monomer and organic crosslinker for the hydrogelation, the *G*' and *G*" values are readily modulable in a certain range without deteriorating the anisotropic mechanical feature (Supplementary Fig. 16). Also noteworthy, our hydrogel, just like polymer electrolyte hydrogels[30], is protected against ion penetration (Supplementary Fig. 17) and, upon immersion in physiological saline, its mechanical anisotropy is hardly lost for a rather long period of time (Supplementary Fig. 18).

References

1. Hull, J. R. Superconducting bearings. *Supercond. Sci. Technol.* **13**, R1–R15 (2000).

2. Rhim, W. K. *et al.* An electrostatic levitator for high-temperature containerless materials processing in 1-G. *Rev. Sci. Instrum.* **64**, 2961–2970 (1993).

3. Scott, J. E. Elasticity in extracellular matrix ‘shape modules’ of tendon, cartilage, *etc.* A sliding proteoglycan-filament model. *J. Physiol.* **553**, 335–343 (2003).

4. Dean, D., Han, L., Grodzinsky, A. J. & Ortiz, C. Compressive nanomechanics of opposing aggrecan macromolecules. *J. Biomech.* **39**, 2555–2565 (2006).

5. Sasaki, T., Watanabe, M., Hashizume, H., Yamada, H. & Nakazawa, H. Macromolecule-like aspects for a colloidal suspension of an exfoliated titanate. Pairwise association of nanosheets and dynamic reassembling process initiated from it. *J. Am. Chem. Soc.* **118**, 8329–8335 (1996).

6. Anandarajah, A. & Ning, L. Numerical study of the electrical double-layer repulsion between nonparallel clay particles of finite length. *Int. J. Numer. Anal. Met.* **15**, 683–703 (1991).

7. Cui, H. G. *et al.* Spontaneous and X-ray-triggered crystallization at long range in self-assembling filament networks. *Science* **327**, 555–559 (2010).

8. Palmer, L. C. *et al.* Long-range ordering of highly charged self-assembled nanofilaments. *J. Am. Chem. Soc.* DOI: 10.1021/ja5082519 (2014).

9. Wu, Z. L. *et al.* Anisotropic hydrogel from complexation-driven reorientation of semirigid polyanion at Ca^{2+} diffusion flux front. *Macromolecules* **44**, 3535–3541 (2011).

10. Wu, J., Zhao, Q., Sun, J. & Zhou, Q. Preparation of poly(ethylene glycol) aligned porous cryogels using a unidirectional freezing technique. *Soft Matter* **8**, 3620–3626 (2012).

11. Liu, M., Ishida, Y., Ebina, Y., Sasaki, T. & Aida, T. Photolatently modulable hydrogels using unilamellar titania nanosheets as photocatalytic crosslinker. *Nat. Commun.* **4**, 2029-1–7 (2013).

12. Eguchi, M., Angelone, M. S., Yennawar, H. P. & Mallouk, T. E. Anisotropic alignment of lamellar potassium hexaniobate microcrystals and nanoscrolls in a static magnetic field. *J. Phys. Chem. C.* **112**, 11280–11285 (2008).

13. Ida, S. *et al.* Photoluminescence of perovskite nanosheets prepared by exfoliation of layered oxides, K(2)Ln(2)Ti(3)O(10), KLnNb(2)O(7), and RbLnTa(2)O(7) (Ln: lanthanide ion). *J. Am. Chem. Soc.* **130**, 7052–7059 (2008).

14. Osada, M. *et al.* Ferromagnetism in two-dimensional $Ti_{0.8}Co_{0.2}O_2$ nanosheets. *Phys. Rev. B* **73**, 153301-1–153301-4 (2006).

15. Prosser, S., Hunt, S. A., DiNatale, J. A. & Vold, R. R. Magnetically aligned membrane model systems with positive order parameter: switching the sign of S_{zz} with paramagnetic ions. *J. Am. Chem. Soc.* **118**, 269–270 (1996).

16. Tan, C., Fung, B. M. & Cho, G. Phospholipid bicelles that align with their normals parallel to the magnetic field. *J. Am. Chem. Soc.* **124**, 11827–11832 (2002).

17. Kleinschmidt, F., Hickl, M., Saalwächter, K., Schmidt, C. & Finkelmann, H. Lamellar liquid single crystal hydrogels: synthesis and investigation of anisotropic water diffusion and swelling. *Macromolecules* **38**, 9772–9782 (2005).

18. Haque, M. A., Kamita, G., Kurokawa, T., Tsujii, K. & Gong, J. P. Unidirectional alignment of lamellar bilayer in hydrogel: one-dimensional swelling, anisotropic modulus, and stress/strain tunable structural color. *Adv. Mater.* **22**, 5110–5114 (2010).

19. Erb, R. M., Libanori, R., Rothfuchs, N. & Studart, A. R. Composites reinforced in three dimensions by using low magnetic fields. *Science* **335**, 199–204 (2012).

20. Wang, Q. *et al.* High-water-content mouldable hydrogels by mixing clay and a dendritic molecular binder. *Nature* **463**, 339–343 (2010).

21. Tamesue, S. *et al.* Linear versus Dendritic molecular binders for hydrogel network formation with clay nanosheets: studies with ABA triblock copolyethers carrying guanidinium ion pendants. *J. Am. Chem. Soc.* **135**, 15650−15655 (2013).

22. Maret, G. & Dransfeld, K. Biomolecules and polymers in high steady magnetic fields. *Top. Appl. Phys.* **57**, 143–204 (1985).

23. Löwen, H. Colloidal soft matter under external control. *J. Phys. Condens. Matter.* **13**, R415–R432 (2001).

24. Uyeda, C. *Phys. Chem. Miner.* Diamagnetic anisotropies of oxide minerals. **20**, 77–81 (1993).

25. Torbet, J., Freyssinet, J. M. & Hudry-Clergeon, G. Oriented fibrin gels formed by polymerization in strong magnetic fields. *Nature* **289**, 91–93 (1981).

26. Feng, S. *et al.* Hierarchical structure in oriented fibers of a dendronized polymer. *Macromolecules* **42**, 281–287 (2009).

27. Verwey, E. J. W. & Overbeek, J. Th. G. *Theory of the Stability of Lyophobic Colloids* (Elsevier, Amsterdam, 1948).

28. Podsiadlo, P. *et al.* Ultrastrong and stiff layered polymer nanocomposites. *Science* **318**, 80–83 (2007).

29. Munch, E. *et al.* Tough, bio-inspired hybrid materials. *Science* **322**, 1516–1520 (2008).

30. Budtova, T. & Navard, P. Swelling-induced birefringence of a polyelectrolyte gel strongly interacting with metal ions. *Macromolecules* **30**, 6556–6558 (1997).

Supplementary Information is available in the online version of the paper.

Acknowledgements

This work was financially supported by Grant-in-Aid for Specially Promoted Research (25000005) on “Physically Perturbed Assembly for Tailoring High-Performance Soft Materials with Controlled Macroscopic Structural Anisotropy”. We also acknowledge ImPACT Program of Council for Science, Technology and Innovation (Cabinet Office, Government of Japan). The synchrotron X-ray diffraction experiments were performed at BL45XU in SPring-8 with the approval of RIKEN SPring-8 Center (proposal 20140073).

Author contributions

M.L. designed and performed all experiments. Y.I. and T.A. co-designed the experiments. Y.E. and T.S. prepared colloidally dispersed TiNSs and NbNSs. M.L., Y.I. and T.A. analyzed the data and wrote the manuscript. T.H. and M.T. supported the XRD measurements at SPring-8.

Author information

Reprints and permissions information is available at www.nature.com/reprints. The authors declare no competing financial interests. Readers are welcome to comment on the online version of the paper. Correspondence and requests for materials should be addressed to Y.I. (y-ishida@riken.jp) or T.A. (aida@macro.t.u-tokyo.ac.jp).

Figure legends

Figure 1 | Negatively charged unilamellar metal oxide nanosheets of titanate (TiNS) and niobate (NbNS). **a**, Metal oxide nanosheets in close proximity to one another are electrostatically repulsive. When two nanosheets are positioned at a fixed distance, the repulsive force changes with their dihedral angle, where cofacial (dihedral angle = 0°; left) and orthogonal (dihedral angle = 90°; right) nanosheet orientations provide the maximum and minimum repulsive forces, respectively. **b**, **c**, Schematic structures of TiNS (**b**) and NbNS (**c**) negatively charged having tetramethylammonium (Me_4N^+) counterions. **d**, Elementary steps for photoinduced hydrogelation at 25 °C by using crosslinking polymerization of a mixture of

mono- and difunctional acrylamide derivatives (iii and iv) initiated by hydroxyl radicals, in-situ generated upon photoexcitation of TiNS (i and ii) in aqueous media.

Figure 2 | Magnetic responses of unilamellar metal oxide nanosheets of titanate (TiNS) and niobate (NbNS). **a**, TiNSs orient their 2D plane orthogonal to an applied magnetic flux, so that they are cofacial. The optical transmittance along the magnetic flux is smaller than that in its orthogonal direction. **b**, NbNSs direct their orientation vector parallel to an applied magnetic flux, and are freely rotatable around the orientation vector. The optical transmittance along the magnetic flux is larger than that in its orthogonal direction. **c**, **d**, Optical transmittances at 450 nm of aqueous colloidal dispersions of TiNSs (**c**) and NbNSs (**d**) (0.4 wt%) upon orthogonal (⊥) and parallel (//) directions of a 10-T magnetic flux to the incident light. For optical measurements, the dispersions contained 8.0 wt% poly(*N*,*N*-dimethylacrylamide) as a thickener. Broken lines represent optical transmittances of the dispersions without magnetic flux.

Figure 3 | Structural and optical anisotropic features of hydrogels containing cofacially oriented TiNSs in a quasi-crystalline order. **a**, Spatial immobilization of cofacially oriented TiNSs by hydrogelation with TiNS-mediated photoinduced crosslinking polymerization (Fig. 1d) in a 10-T magnetic flux. **b**, Optical features of the resultant hydrogel (TiNS; 0.4 wt%) viewed along orthogonal (i) and parallel (ii, iii) directions to the magnetically oriented TiNS plane. **c**, 2D small-angle X-ray scattering (SAXS) images of the resultant hydrogel (TiNS; 0.6 wt%), where the incident X-ray beam was directed orthogonal (i) and parallel (ii) to the magnetically oriented TiNS plane. **d**, **e**, Effects of [TiNS] at a constant Me_4N^+/TiNS ratio (13 mM/0.1 wt%) (**d**) and of [Me_4NOH]* at a constant [TiNS] (0.8 wt%) (**e**) on 1D SAXS (insets: *d*-spacings of TiNSs) profiles of hydrogels prepared with

various amounts of TiNS and Me_4NOH. In the insets of **d** and **e**, each point represents a single measurement.

Figure 4 | Mechanical anisotropy of hydrogels containing cofacially oriented TiNSs in a quasi-crystalline order. **a**, **b**, Schematic representations for mechanical deformations of a hydrogel containing cofacially oriented TiNSs (Fig. 1d) sheared (**a**) and compressed (**b**) in orthogonal (⊥; left) and parallel (//; right) directions to the TiNS plane. **c**, Strain–stress curves of a hydrogel (TiNS; 0.8 wt%) with applied compression strain (ε) = 0–50% at a constant compression rate of 20% min^{-1}. **d**, Storage moduli (G') of a hydrogel (TiNS; 0.8 wt%) on frequency (ω) sweep in a range of 0.1–7.5 rad s^{-1} at a constant shear strain (γ) of 0.5%. **e**, **f**, Effects of [TiNS] on tangent elastic moduli (E) at ε = 40% (**e**) and storage moduli (G') at ω = 1.33 rad s^{-1} (**f**), where each point represents a single measurement. In **c**–**f**, mechanical properties in blue and pink colors were obtained when the hydrogels were deformed in orthogonal (⊥) and parallel (//) directions to the magnetically oriented TiNS plane, respectively. **g**, **h**, Demonstrations of vibration isolation. On a mechanical oscillator, a glass stage featuring a metal sphere on a tee was supported by three cylindrical pillars of magnetically structured hydrogel containing cofacially oriented TiNSs (0.8 wt%) in parallel (**g**) or orthogonal (**h**) direction to the cylinder cross-section.

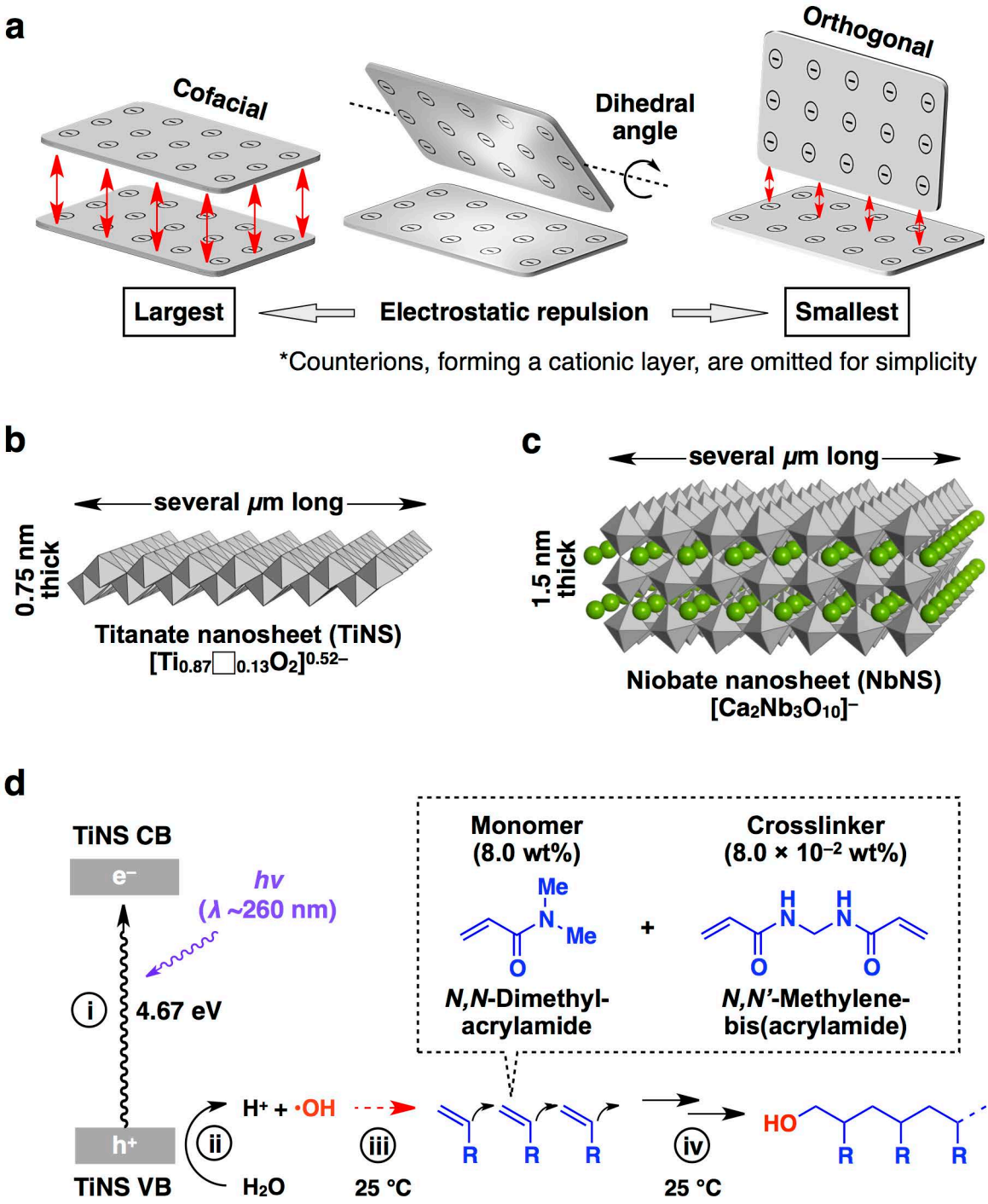
a
Cofacial
Dihedral angle
Orthogonal
Largest
Electrostatic repulsion
Smallest
*Counterions, forming a cationic layer, are omitted for simplicity
b
several μm long
0.75 nm thick
Titanate nanosheet (TiNS)
[Ti0.87□0.13O2]0.52–
c
several μm long
1.5 nm thick
Niobate nanosheet (NbNS)
[Ca2Nb3O10]–
d
TiNS CB
e–
hν
(λ ~260 nm)
i
4.67 eV
h+
TiNS VB
ii
H+ + ·OH
H2O
iii
25 °C
Monomer
(8.0 wt%)
Crosslinker
(8.0 × 10–2 wt%)
Me
N
Me
O
+
H
N
H
N
O
O
N,N-Dimethyl-
acrylamide
N,N'-Methylene-
bis(acrylamide)
R
R
R
iv
25 °C
HO
R
R
R

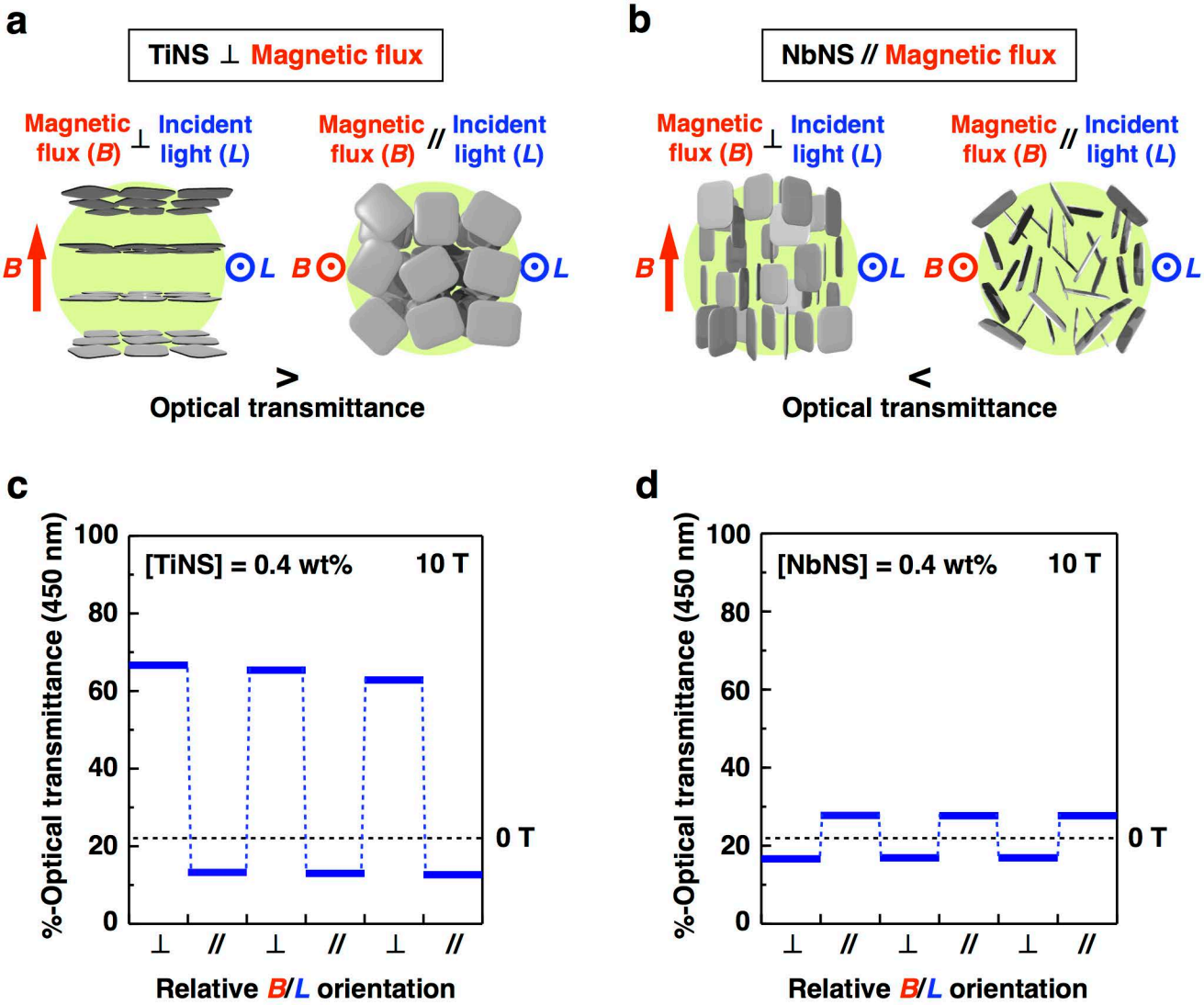
a
TiNS ⊥ Magnetic flux
Magnetic flux (B) ⊥ Incident light (L)
Magnetic flux (B) // Incident light (L)
B
L
B
L
>
Optical transmittance
b
NbNS // Magnetic flux
Magnetic flux (B) ⊥ Incident light (L)
Magnetic flux (B) // Incident light (L)
B
L
B
L
<
Optical transmittance
c
[TiNS] = 0.4 wt%
10 T
0 T
%-Optical transmittance (450 nm)
100
80
60
40
20
0
⊥ // ⊥ // ⊥ //
Relative B/L orientation
d
[NbNS] = 0.4 wt%
10 T
0 T
%-Optical transmittance (450 nm)
100
80
60
40
20
0
⊥ // ⊥ // ⊥ //
Relative B/L orientation

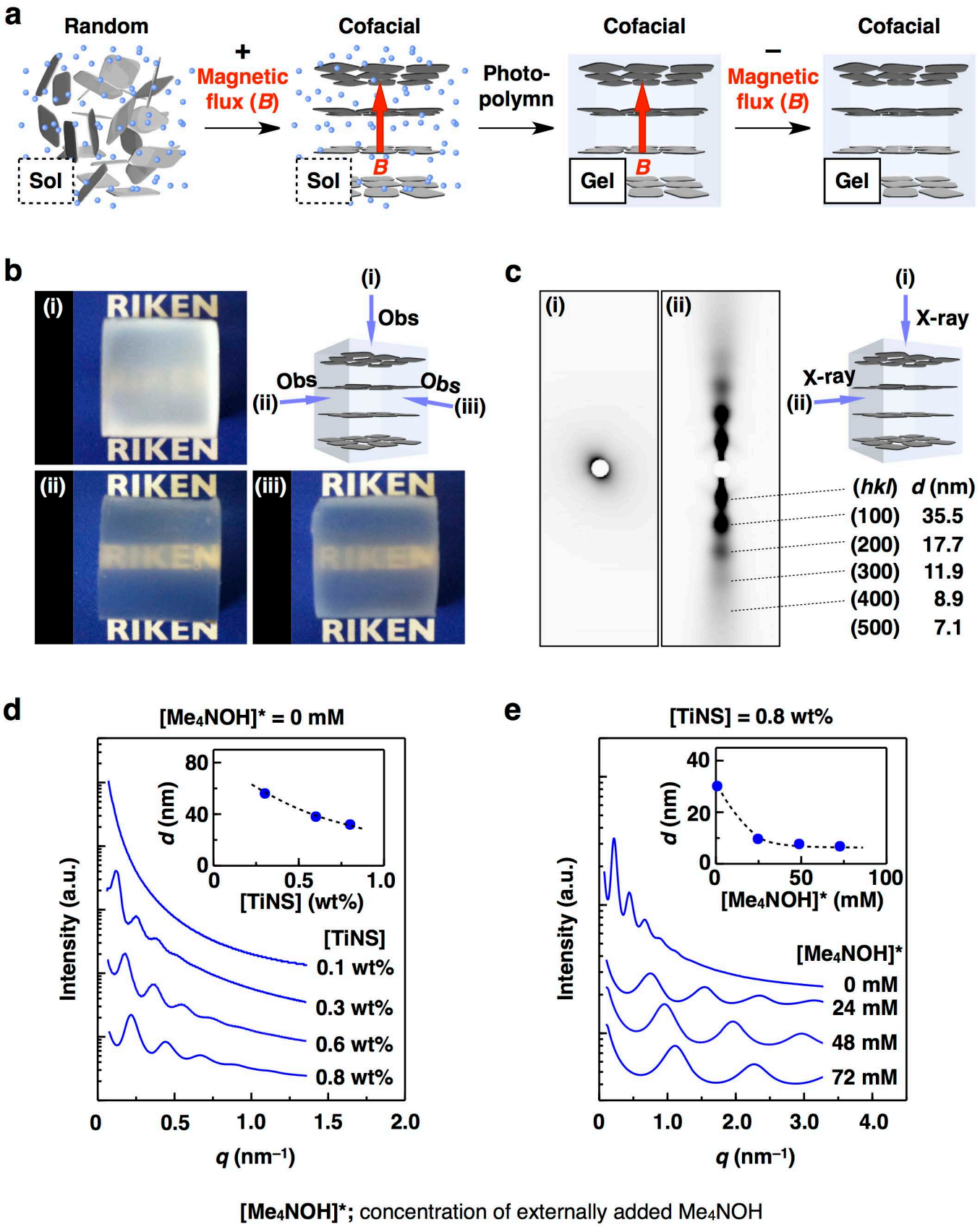

[Me4NOH]*; concentration of externally added Me4NOH

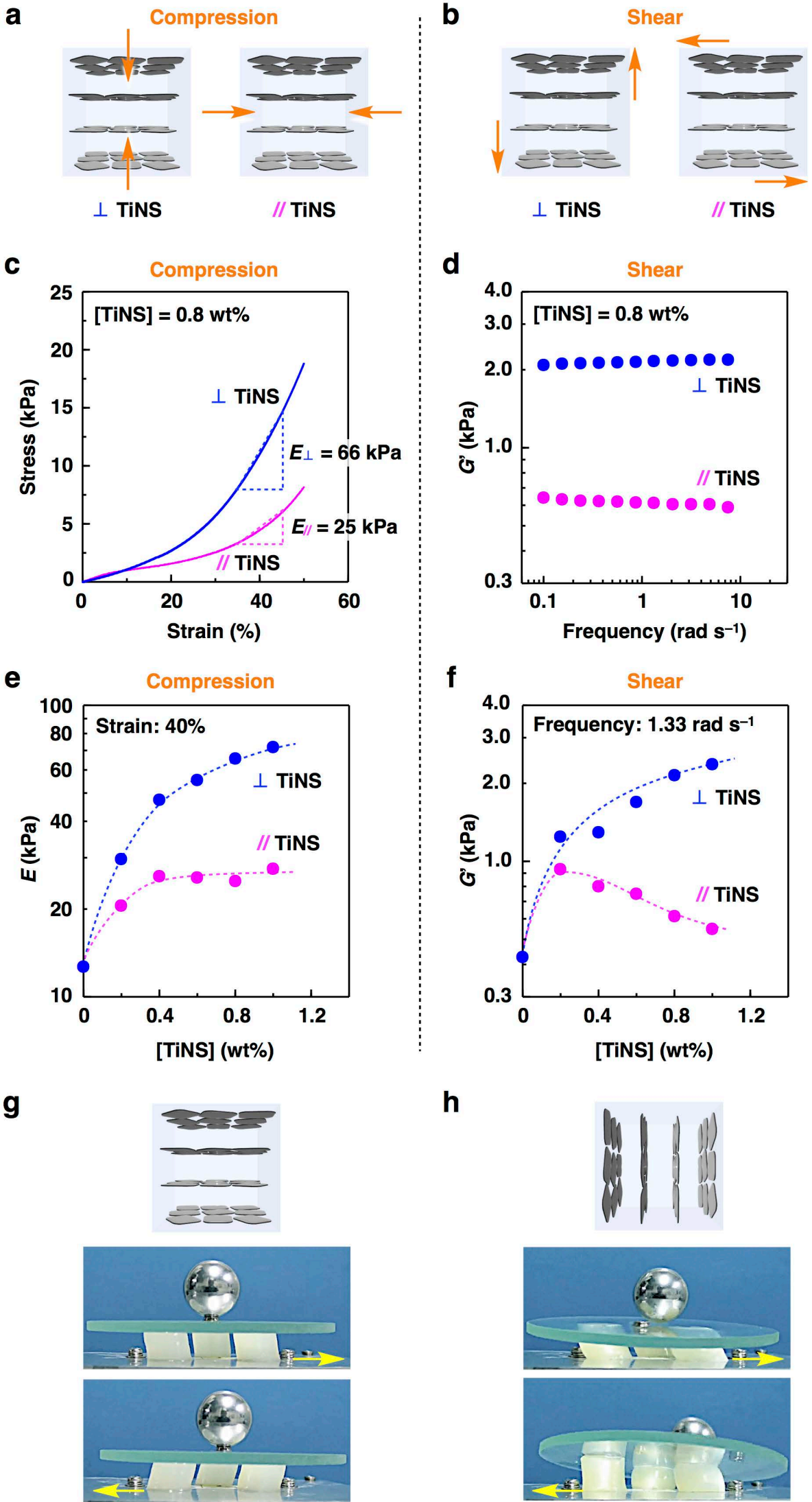
a
Compression
⊥ TiNS
// TiNS
b
Shear
⊥ TiNS
// TiNS
c
Compression
[TiNS] = 0.8 wt%
⊥ TiNS
E⊥ = 66 kPa
E// = 25 kPa
// TiNS
Stress (kPa)
Strain (%)
d
Shear
[TiNS] = 0.8 wt%
⊥ TiNS
// TiNS
G' (kPa)
Frequency (rad s−1)
e
Compression
Strain: 40%
⊥ TiNS
// TiNS
E (kPa)
[TiNS] (wt%)
f
Shear
Frequency: 1.33 rad s−1
⊥ TiNS
// TiNS
G' (kPa)
[TiNS] (wt%)
g
h